Novel technique for measuring the mechanical properties of porous materials by nanoindentation

Xi Chen[a)]
Department of Civil Engineering and Engineering Mechanics, Columbia University, New York, New York 10027-6699

Yong Xiang and Joost J. Vlassak
Division of Engineering and Applied Sciences, Harvard University, Cambridge, Massachusetts 02138-2901

(Received 4 August 2005; accepted 8 December 2005)

A new technique for measuring the elastic-plastic properties of porous thin films by means of nanoindentation is proposed. The effects of porosity on indentation hardness and modulus are investigated through finite element analyses based on the Gurson model for plastic deformation of ductile porous materials. Intrinsic mechanical properties of the thin film are obtained by eliminating both substrate and densification effects. The technique is applied to the special case of a porous, low-permittivity dielectric thin film. The results are in good agreement with those obtained independently using the plane-strain bulge test.

I. INTRODUCTION

A. Motivation

The mechanical response of thin films can be measured using many different techniques, including microtensile or bulge testing of free-standing thin films,[1–3] nanoindentation, the micro-beam cantilever deflection technique,[4,5] and the substrate curvature technique.[6,7] Compared to other methods, nanoindentation measurements can be made without having to remove the film from its substrate; moreover, nanoindentation is an isothermal technique that does not require thermal cycling. It is perhaps the quickest and easiest method for probing the mechanical properties of thin films. Special care is required, however, when nanoindentation is performed on porous materials. Because of their porous microstructure, the response of these materials during a nanoindentation experiment is very different from that of a dense bulk material. In this paper, we investigate the mechanics of nanoindentation of porous materials and develop a new technique to correlate the experimental data with the inherent microstructure and mechanical properties of these materials. The approach advanced in this paper is applied to the special case of a porous polymeric thin film used as a low-k dielectric in the microelectronics industry, but it is readily extended to other porous materials with relatively low pore density (<30%) such as sintered materials, thermal-barrier coatings, or biological materials such as bone.

B. Brief review of nanoindentation of bulk materials

The analysis of nanoindentation experiments on elastic-perfectly plastic, homogeneous bulk materials[8–11] is well developed and is briefly reviewed in this subsection. Instrumented indentation is characterized by a rigid indenter (with angle α) penetrating normally into a homogeneous solid while the indentation load P and displacement δ are continuously recorded during one complete cycle of loading and unloading (Fig. 1). The indenter most commonly used in nanoindentation experiments is the Berkovich tip, i.e., a three-sided pyramidal tip with the same cross-sectional area-to-depth ratio as the Vickers indenter. To simplify the analysis, the indenter is usually modeled as an axisymmetric rigid cone with $\alpha = 19.7°$, so that the ratio of area to depth is the same as for a Berkovich or Vickers indenter.[12] If friction and the finite compliance of the measuring system and the indenter tip are neglected, the equations to extract the hardness H and indentation modulus M of the bulk material are

$$H = P/A \quad , \tag{1}$$

and

$$S = \gamma \frac{2}{\sqrt{\pi}} M\sqrt{A} \quad . \tag{2}$$

Here, the hardness H is defined as the ratio between indentation load P and projected contact area A. The

[a)]Address all correspondence to this author.
e-mail: xichen@civil.columbia.edu
DOI: 10.1557/JMR.2006.0088

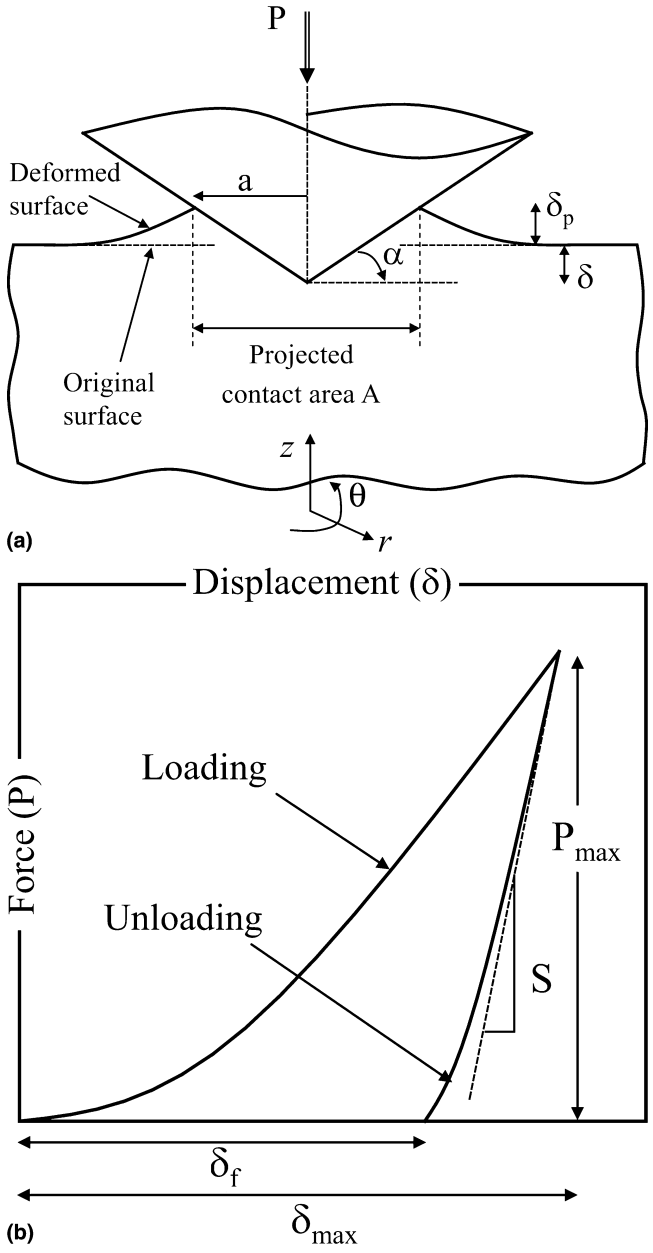

FIG. 1. (a) Schematic illustration of conical (Berkovich) indentation on a homogeneous, isotropic, semi-infinite substrate; (b) typical load–displacement curve obtained from experiment.

contact stiffness $S = dP/d\delta$ is obtained from the slope of the initial portion of the elastic unloading curve [Fig. 1(b)]; $\gamma \approx 1.08$ is a correction factor for the Berkovich indenter.[13,14] For homogeneous, elastic-perfectly plastic bulk materials, the bulk hardness H_b is proportional to the material yield stress σ_y, and the bulk indentation modulus M_b equals the plane-strain modulus of the bulk specimen, respectively given by

$$H_b = c_o\sigma_y \quad , \tag{3}$$

and

$$M_b = \bar{E} \equiv E/(1 - \nu^2) \quad , \tag{4}$$

where E and ν are Young's modulus and Poisson's ratio of the isotropic bulk material, respectively. For anisotropic materials, M_b is given by a complicated function of the elastic constants.[15] The constant c_b in Eq. (3) is a constraint factor that depends on indenter shape and material properties: c_b increases with E/σ_y and approaches a constant value (~3) when $\bar{E}\tan\alpha/\sigma_y > 30$.[12,14] If the material work hardens, the yield stress is taken at a representative strain,[16] which is approximately 7% for a Berkovich indenter.

As the indenter penetrates the specimen, the material exhibits both elastic sink-in and plastic pile-up at the edge of the indentation. The elastic effect is more pronounced when the yield strain of the material σ_y/E is large; plastic pileup is important for materials with a small yield strain.[14] The amount of pileup/sink-in is denoted as δ_p [Fig. 1(a)]. For the axisymmetric Berkovich indenter, the projected contact area A is given by:

$$A = \pi a^2 = \pi(\tan\alpha)^2\delta_c^2 = 24.5\delta_c^2 \quad , \tag{5}$$

where the contact depth,

$$\delta_c = \delta + \delta_p \quad . \tag{6}$$

Equation (6) contains contributions of both plastic pileup around the indenter and elastic sink-in, which is counted negative. It is obvious from Eqs. (1)–(6) that the accuracy of the hardness and stiffness measurements depends on the accuracy with which A (or δ_p) can be determined experimentally. Oliver and Pharr[8] proposed an elastic model in which plastic pileup is neglected, to determine the contact area:

$$|\delta_p| = \eta P_{max}/S_{max} \quad , \tag{7}$$

where $\eta = 0.75$ for a conical indenter. This equation is widely used in the analysis of nanoindentation data, including the analysis of the experimental data presented in this study. Alternatively, the pileup and projected contact area can be measured using atomic force microscopy. Once A is determined properly, the elastic-plastic properties $\bar{E}$ and σ_y are obtained from Eqs. (3) and (4).

C. Effect of the Substrate

For thin film/substrate systems, a systematic investigation of the substrate effect in nanoindentation was performed by Chen and Vlassak[14] using the finite element analysis. To make the connection with the porous low-k dielectric film investigated in the companion paper[24] and used as an example in this paper, only selected results for soft compliant films on hard and stiff substrates are reviewed in this section. [For other cases where the film may be stiffer and/or harder than the substrate, e.g. thermal-barrier coatings, the substrate effect may also be

eliminated using the techniques proposed by Chen and Vlassak.[14]] For hardness measurements, it is found that the substrate effect is relatively small as long as the indentation depth is smaller than 50% of the film thickness (h). That is, when $\delta < h/2$, the experimental hardness $H = P/A$ is approximately the same as that of the thin film material, $H_b = c_b\sigma_y^f \approx H$ [Fig. 2(a)].[14] If the indentation depth increases beyond 50% of the film thickness, H increases and quickly approaches the substrate hardness. In this case, using $\sigma_y^f = H/c_b$ to obtain the film yield stress from the measurement would result in a significant error; Chen and Vlassak[14] have developed a hardness correction map that makes it possible to eliminate the substrate effect at a given indentation depth. Hardness measurements are governed mainly by the yield stress mismatch between the film and substrate σ_y^f/σ_y^s and are essentially independent of the elastic mismatch E^f/E^s.

For thin film stiffness measurements, by contrast, the substrate effect is significant even for small contact areas [Fig. 2(b), redrawn based on the data in Ref. 14]. Here, $E_{eff} = \sqrt{\pi}S(1-\nu^2)/(2\gamma\sqrt{A})$ is the effective modulus calculated from Eq. (2). The substrate effect is not negligible and E_{eff} is larger than the real modulus of the film E^f, even if the indentation depth is just 10% of the film thickness. Moreover, E_{eff} increases rapidly and approaches the substrate modulus E^s with increasing δ. The stiffness measurement is affected only by the size of the contact area and the elastic mismatch E^f/E^s. Figure 2(b) serves as a thin film stiffness correction map, which represents the substrate stiffness effect as a function of film/substrate mismatch and indentation depth; along with the hardness correction map,[14] it may be used to obtain the intrinsic properties of a film by eliminating the substrate effect. The results compiled in Figs. 2(a) and 2(b) agree well with experimental results.[17]

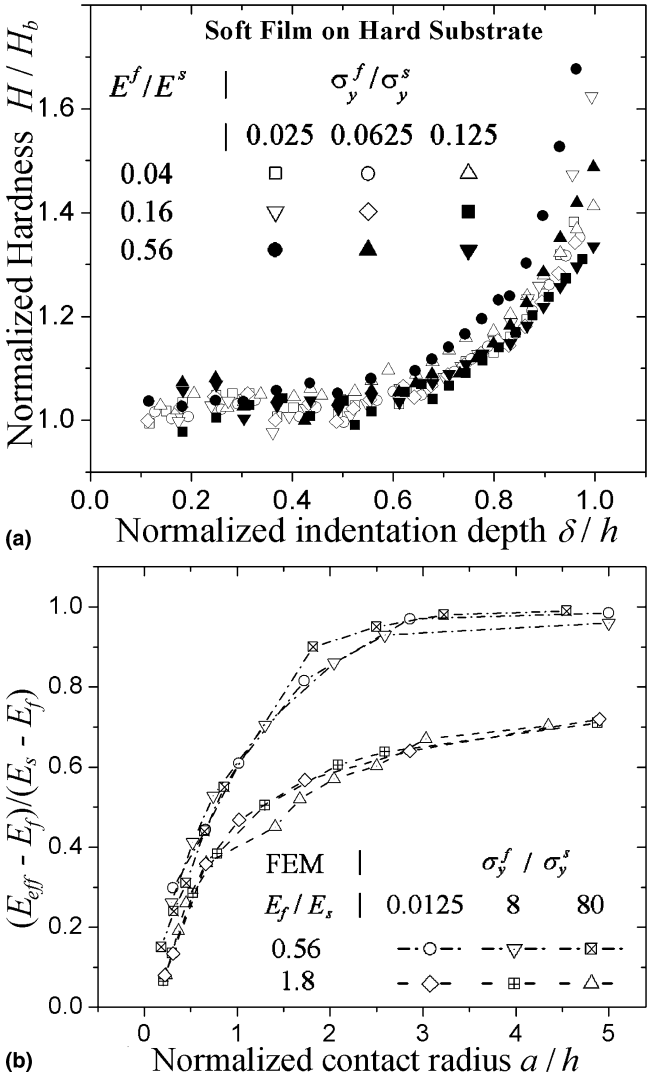

FIG. 2. Substrate effect for a soft film deposited on a hard substrate:[14] (a) substrate effect on measured hardness; (b) substrate effect on measured stiffness as a function of normalized contact radius, assuming Poisson's ratios are identical.

D. Effect of porosity

For a porous material, both the elastic modulus E^P and the yield stress σ_y^P are functions of the porosity f of the material, which in turn depends on the deformation history of the material. Fleck et al.[18] studied the effect of porosity on indentation of bulk materials with known elastic modulus and porosity using both the finite element analysis and a cavity expansion model. These authors suggest that the resistance to indentation increases with decreasing initial porosity. The deformation fields obtained using the finite element method agree well with experimental observations for sintered steels. Recently, Volinsky et al.[19] measured the mechanical properties of porous low-k dielectric films using nanoindentation. They found that both indentation modulus and hardness increase with penetration depth as a result of densification of the material and the presence of the substrate. Their observations are in general agreement with indentation analyses on other porous materials such as thermal-barrier coatings.[20–22] These studies suggest that local densification of the porous material is important during nanoindentation: the intrinsic, elastic-plastic properties (E^P, σ_y^P) of the porous film cannot be derived directly from the classic formulae (3) and (4).

The question then arises if it is possible to measure intrinsic mechanical properties of porous materials using nanoindentation. How does porosity affect hardness and indentation modulus? These are questions that will be explored in detail in this study. Unlike the forward analysis by Fleck et al.,[18] in the work presented here we carry out an inverse analysis, focusing on the extraction of intrinsic material properties from nanoindentation experiments on porous materials.

The paper is organized as follows. We first give an overview of the nanoindentation experiments performed on both fully dense and porous polymeric films. A finite element analysis is used to simulate the nanoindentation experiments. This analysis employs the Gurson model[23] to characterize plastic deformation in the porous solid and to evaluate the effect the porous microstructure. A novel approach is then proposed to extract intrinsic mechanical properties of the porous films from the nanoindentation load–displacement curves. This new approach is applied to porous thin films, and the results are compared with independent measurement obtained using the plane-strain bulge test.

II. EXPERIMENT

This section summarizes the results of an experimental study[24] in which the mechanical properties of both a fully dense and a porous low-k dielectric thin film were measured using two different techniques: nanoindentation and the plane-strain bulge test. The detailed experimental procedure and analysis can be found in Ref. 24.

Nanoindentation experiments were performed on two polymer films on silicon substrates using a Nanoindenter XP (MTS, Oak Ridge, TN) with a Berkovich tip. The first film was a fully dense, poly-aromatic film; the second film consisted of the same polymer but with a porosity of 23% as measured by means of x-ray porosimetry. Both films were 850 nm thick. The nanoindenter was operated in the continuous stiffness mode (CSM) in which a small oscillation is superposed on the indentation load. This mode of operation allows the modulus and hardness to be continuously determined as a function of the indentation depth, as presented in Figs. 3(a)–3(b). It is evident from the figures that the experimental values of stiffness and hardness increase with increasing indentation depth. This trend is usually ascribed to the presence of a hard and stiff substrate and/or densification of the material underneath the indenter. It is generally assumed that substrate effects become insignificant when the indentation depth is less than 10% of the film thickness.[25] The results in Fig. 3(a) show that the experimental values of the indentation moduli continue to decrease more slowly at these shallow depths. The intrinsic indentation moduli were estimated by taking the value at an indentation depth of 5% of the film thickness. The hardness data in Fig. 3(b) follow the same trend as the indentation moduli. The figures also give a good indication of the effect of the porosity on the behavior of the films. Introduction of 23% porosity in the polymer films causes a reduction of the elastic modulus by approximately 29% and a reduction of the hardness by roughly 32%. The nanoindentation results are summarized in Table I.

The mechanical response of the polymer films was also measured independently using the plane-strain bulge test.[2,3] Long rectangular membranes were fabricated out of both fully dense and porous polymer films using Si micromachining techniques. The membranes were deformed in plane strain by applying a uniform pressure to the membranes while measuring their deflection. The applied pressure and the corresponding membrane deflection can be converted directly into the plane-strain stress-strain curves of the films.[2,3,24] The plane-strain moduli of the films $M = E/1 - \nu^2$) were determined from linear fits to the initial elastic sections of the stress-strain curves and are listed in Table I. For comparison with the nanoindentation measurements, the representative flow stresses of the polymer films are also tabulated. Since all membranes broke at strains less than 7%, the rupture

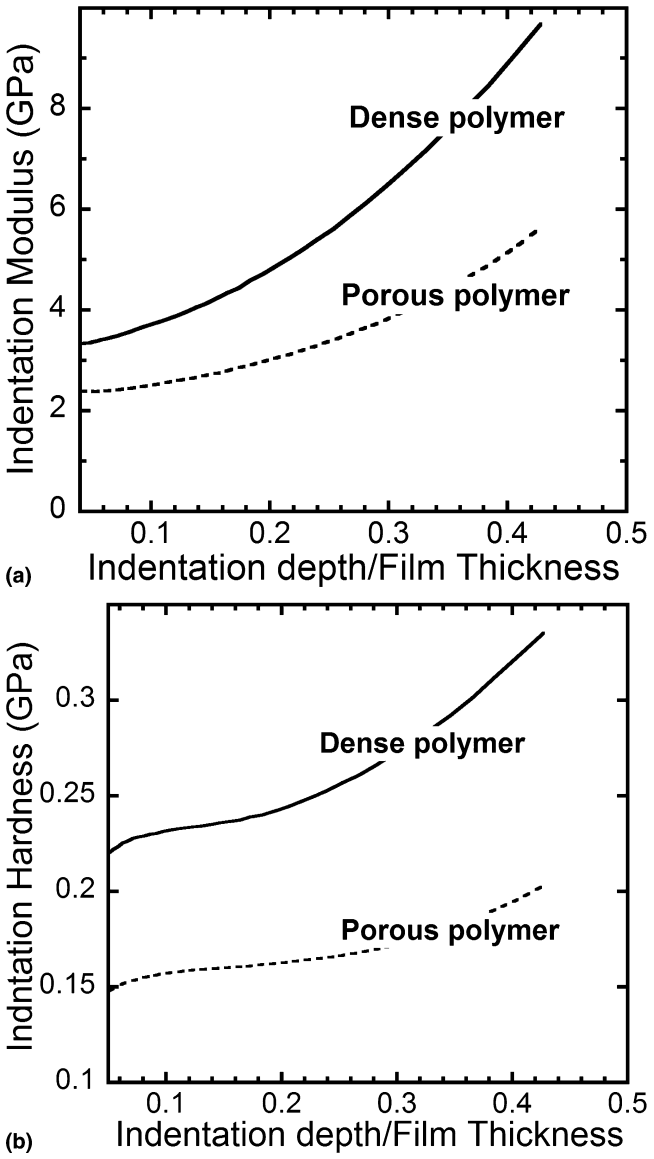

FIG. 3. Comparison of (a) the indentation modulus and (b) the hardness as a function of the normalized indentation depth for porous and fully dense polymer films.[24]

TABLE I. Summary of the experimental results for the polymer films.[24]

	Plane-strain modulus (GPa)			Strength (MPa)		
		Nanoindentation			Nanoindentation	
Film type	Bulge test	Measured	Corrected[a]	Bulge test σ_y	Hardness[b]	σ_y
Fully dense	2.7 ± 0.1	3.4 ± 0.2	2.7 ± 0.2	93 ± 4	231 ± 5	115 ± 3
23% porosity	2.0 ± 0.1	2.4 ± 0.3	1.9 ± 0.3	>55 ± 3[c]	158 ± 5	86 ± 3

[a]Results corrected for the presence of the substrate for an indentation depth of 5% of the film thickness.
[b]Hardness values are taken at an indentation depth of 10% of the film thickness.
[c]Stress at film rupture, films failed in the elastic regime without obvious plastic deformation.

stresses of the membranes were taken to be the representative flow stresses. These values should therefore be regarded as lower bounds to the actual flow stresses.

III. FINITE ELEMENT ANALYSIS

A. Finite element modeling

Because there is no analytical solution to the elastic-plastic indentation problem, the finite element method (FEM) was used to investigate the effect of porosity and densification on the mechanical property measurements for a range of porous materials. The finite element method is useful for this purpose because it provides a convenient way of measuring the projected contact area between indenter and material needed for calculation of hardness and stiffness. It is straightforward to vary material properties over a wide range, and the analysis also provides direct information on the pile-up height through an analysis of the surface contour during the indentation process.

Finite element calculations were performed using the commercial code ABAQUS.[26] The rigid contact surface option was used to simulate the Berkovich indenter, and the option for finite deformation and strain was used. A typical mesh for the axisymmetric indentation model comprises more than 10,000 8-node elements with reduced integration. To ensure convergence for shallow indentations, the tip of the indenter was assumed to be rounded with a radius of curvature of 60 nm. Coulomb's friction law was used between contact surfaces. The friction coefficient was taken to be 0.1, but the precise value of the friction coefficient has very little influence on the results.[27] The projected contact area was calculated directly from the numerical results by analyzing the nodes in contact with the indenter.

The Gurson model[23] for plastic deformation of porous ductile materials was used as a constitutive law to simulate densification of the material. This model describes the plastic behavior of porous ductile materials with dilute void concentrations (i.e., porosity levels of less than 30%). It has been used in numerical simulations of high-temperature impact and indentation of thermal-barrier coatings (with porosity between 10% and 25%) and agrees well with experimental observations.[20–22] In this model, the matrix material is taken to be a continuum and the effect of the voids is averaged through the elastic-perfectly plastic material. The voids appear in the Gurson model indirectly through the effect of the pore volume fraction f on the global flow behavior. The porosity level evolves with the hydrostatic stress in the porous material: if the hydrostatic stress is tensile, the void volume fraction increases and the material becomes weaker; if the stress is compressive, the void volume fraction decreases and the yield stress of the material increases. The yield condition then takes the form

$$\Phi = \frac{3}{2}\frac{S_{ij}S_{ij}}{(\sigma_y^D)^2} + 2f\cosh\left(\frac{3\sigma_m}{2\sigma_y^D}\right) - [1+f^2] = 0 \quad , \qquad (8)$$

where $\sigma_m = \frac{1}{3}\sigma_{kk}$ is the hydrostatic pressure, $S_{ij} = \sigma_{ij} - \sigma_m$ is the stress deviator, and σ_y^D is the uniaxial yield stress of the fully dense matrix in absence of voids. The rate of change of the void volume fraction is determined from the condition that the matrix material be plastically incompressible. When $f = 0$, the Gurson model reduces to classical J_2-flow theory for dense materials. The yield surface becomes smaller f; i.e., the yield stress of the porous material is smaller than that of its dense counter part, $\sigma_y^P(f) < \sigma_y^D$, with increasing f. It should be noted that the elastic modulus in this finite element analysis was independent of porosity; no variation of stiffness with densification was allowed. This assumption does not affect the results of the analysis very much because the Gurson model is independent of the elastic properties of the solid. The effect of densification on the elastic response of the material is explored in more detail in a later section. The value of Poisson's ratio is a minor factor in indentation studies[27] and is taken to be 0.25 for all materials in this study.

An effective way of handling the substrate effect of nanoindentation on thin films is to calibrate the substrate effect with respect to a reference; i.e., a bulk material with the same properties as the thin film material. The intrinsic properties of this reference material are readily determined from nanoindentation experiments on thin films through use of the classic bulk indentation formulae (1)

and (2) combined with the substrate-correction maps in Fig. 2. The same approach may also be used for indentation of porous materials, as implied by the Gurson model, the reference material in this case is the fully dense phase. Once the mechanical properties of the dense material (i.e., σ_y^D) are determined from nanoindentation experiments, the behavior of its porous counterpart (i.e., σ_y^P) is readily derived from the Gurson model.

B. Numerical results for bulk porous materials

To illustrate the effect of densification, Fig. 4 shows the indentation loading and unloading curves for bulk porous media of varying porosity f, calculated using the Gurson model. It is obvious that for the same penetration depth, the indentation load decreases with increasing porosity due to the presence of voids, i.e., at the same indentation depth the normalized bulk hardness $c_b = H_b/\sigma_y^D$ decreases with increasing porosity. The normalized stiffness $\gamma = S\sqrt{\pi}/2E\sqrt{A} \approx 1.08$ is a depth-independent constant equal to that of the fully dense material. This is so because this analysis does not take into account the variation of elastic modulus with densification and because there is no substrate effect in this case.

A contour plot of the void volume fraction beneath the indenter is given in Fig. 5, where the porosity of the undeformed material is $f = 0.23$. The densification zone is approximately semi-circular with a radius equal to the contact radius. Note that for bulk materials, the only length scale involved is the indentation depth δ at least as long as the indentation depth is much larger than the size of the pores and the radius of curvature of the indenter tip. Self-similarity then dictates that the shape and size of the densification zone in a porous material (compare with Fig. 5) should scale with δ. Therefore, the indenter always probes the same inhomogeneous material, leading to a normalized hardness H_b/σ_y^D that is essentially independent of δ. This is discussed in more detail in Sec. IV.

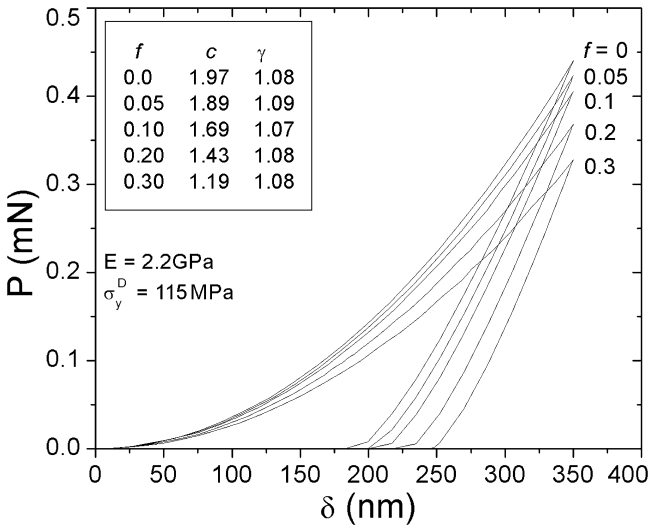

FIG. 4. The effect of porosity on the indentation load-depth curves of bulk specimens as obtained from the FEM model.

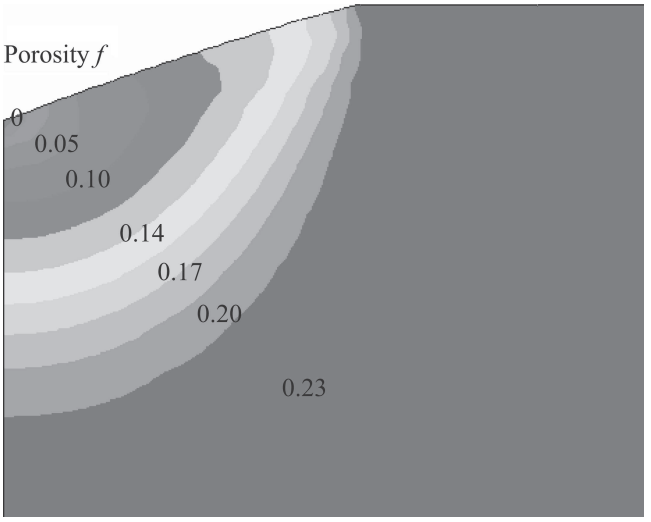

FIG. 5. Typical densification field underneath the conical indenter for materials with an initial porosity of 23%.

C. Numerical results for porous thin films

The indentation depth in the experiments was limited to less than half the film thickness to decouple the substrate effect as much as possible from the densification of the sample. In this section, we present the results of a finite element analysis of these experiments. Indentation of the fully dense material was modeled using standard J_2 flow theory; indentation of the porous material was performed using the Gurson model. In addition to the effect of densification, this analysis also incorporates the substrate effect on the measurements.

In the finite element model of the fully dense polymer film a Young's modulus of 3.1 GPa was used. This value follows from the experimental indentation modulus of this material (Table I) if a Poisson's ratio of 0.25 is assumed. The yield stress of the film, σ_y^D, was varied until the numerical indentation load-depth curve coincided with the experiment data. As illustrated in Fig. 6, very good agreement between experiment and model is obtained for $\sigma_y^D = 115$ MPa (see Fig. 6). The nanoindentation experiment on the porous films was simulated with the Gurson model using Young's modulus of the porous film along with the yield stress of the dense film. The results of the calculation are reported in Fig. 6 together with the experimental results. The agreement between the numerical prediction (open symbols in Fig. 6) and the experimental indentation curve (dashed curve) is outstanding, especially considering that no fitting parameters are involved in the calculation. Clearly,

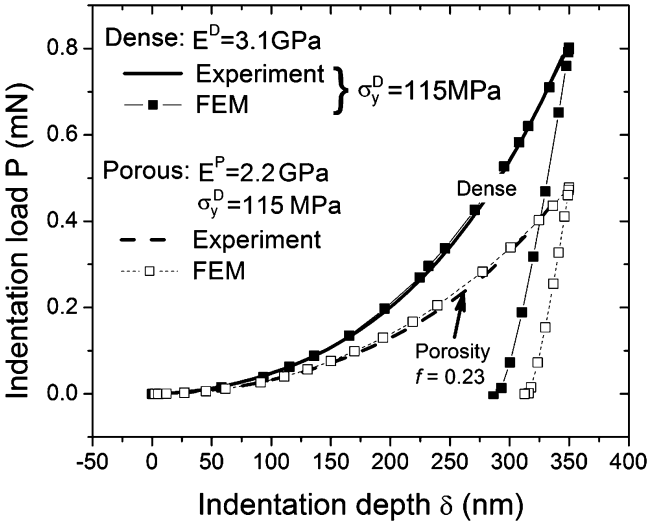

FIG. 6. Experimental and simulated indentation curves for a fully dense and a porous polymeric film. The yield stress of the dense material is used as a fitting parameter for the FEM simulation of the dense material. The FEM indentation curve for the porous material is calculated without any fitting parameters using the Gurson model. The film residual stress is taken to be zero in this case, but the same technique also applies to films with a known level of residual stress.

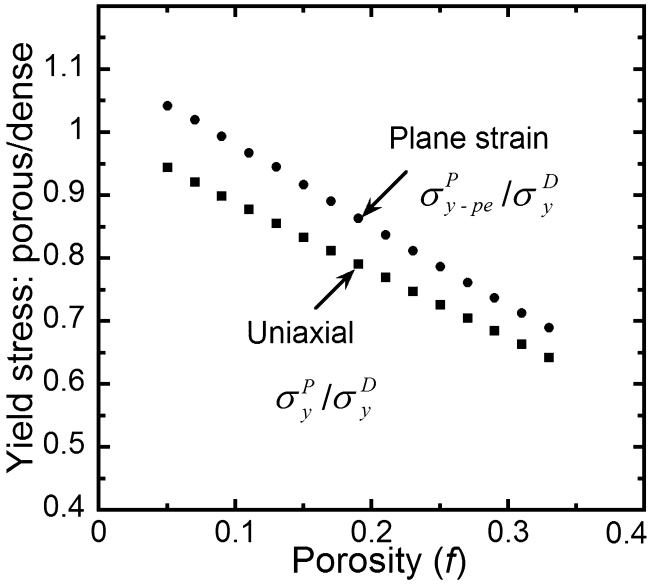

FIG. 7. Conversion map to determine the uniaxial or plane-strain yield stress of a porous material from the yield stress of the fully dense material.

the Gurson model provides a good description for the plastic deformation of porous ductile materials in indentation.

D. Conversion between dense and porous material properties

Analysis of experimental indentation curves using the Gurson model makes it possible to extract the yield stress, σ_y^D, of the fully dense matrix material. For a given porosity, this yield stress, must be converted to the yield stress of the porous material: σ_y^P in uniaxial loading and σ_{y-pe}^P in plane strain, the latter being more useful for comparison with bulge test results later on. Figure 7 shows σ_y^P/σ_y^D and $\sigma_{y-pe}^P/\sigma_y^D$ as a function of porosity: it is evident from the figure that both ratios decrease nearly linearly with increasing porosity, reflecting the reduction in mechanical strength by the introduction of pores into the material. It should be noted that the elastic properties of the material do not enter into the Gurson model, so that the ratio of the flow stresses of a porous and a fully dense material is essentially independent of their yield strains. Analysis of the Gurson yield criterion further shows that the initial yield stress of a porous material is the same in tension and compression.

If the Gurson model is applied to the porous polymer in this study, Fig. 7 yields an estimated yield stress of $\sigma_y^P = 86$ MPa. If the porous structure of the polymer films is ignored and the film is modeled as a homogeneous material using conventional J_2 flow theory, by contrast, an effective yield stress $\sigma_y^{eff} = 53$ MPa is found. The large difference between σ_y^{eff} and σ_y^P demonstrates that it is important to account for local densification underneath the indenter and that the porous structure of the material cannot be ignored. It is therefore inappropriate to treat porous films as homogeneous materials, and new analysis techniques must be developed to extract their intrinsic mechanical properties: For a porous thin film/substrate system with given film thickness and porosity, the dense yield stress σ_y^D can be obtained from an analysis of the experimental data using FEM simulations based on the Gurson model; Fig. 7 is then used to convert σ_y^D into the yield stress of the porous film.

E. Effect of porosity on contact stiffness and modulus

The analysis above requires knowledge of the elastic modulus of the porous film E^P. Unfortunately, the Gurson model alone does not provide information on how densification affects the contact stiffness in an indentation experiment. To evaluate this effect, we have developed a numerical approach based on the fact that deformation during an indentation unloading cycle is essentially elastic. For a bulk material with initial porosity f_0, the porosity field underneath the indenter $[f(r,z)]$ is obtained for a given penetration depth from a Gurson analysis (compare with Fig. 4). This porosity field is then used to determine the contact stiffness from an elastic FEM model in the following fashion: We define a new, inhomogeneous but fully dense material, the stiffness of which depends on the porosity field obtained from the Gurson analysis. More specifically, we assume that Young's modulus of this material at a given location is given by the rule of mixtures $E^D + f(E^P - E^D)/f_0$, where f is the porosity at that location. Thus, if somewhere $f = 0$,

Young's modulus is locally equal to E^D; if $f = f_0$, it is equal to E^P.

Figure 8 shows the elastic indentation curves for several stiffness ratios E^D/E^P and for $f_0 = 0.23$. A reference curve for a homogeneous material with $E^D/E^P = 1$ is also given. It can be concluded that the densification-induced stiffness gradient only plays a role when the elastic properties of the dense and porous phases are very distinct (e.g. $E^D/E^P > 3$). For the polymer films where $E^D/E^P = 1.4$, the difference between the contact stiffness with stiffness gradient and that of the reference curve is less than 1%. The reason for this is that densification is limited to a relatively small region underneath the indenter (Fig. 5), while the region that deforms elastically is much larger than that. Thus, the effect of densification on stiffness measurements is small. This result implies that the rise of the indentation modulus with indentation depth observed in Fig. 3(a) is primarily due to the substrate effect [compare with Fig. 2(b)]. Furthermore, it should be pointed out that it was assumed in the Gurson analysis that the elastic properties of the film were uniform. According to Fig. 8, this assumption is indeed justified for the range of porosities for which the Gurson model holds. In conclusion, nanoindentation is a valid technique for measuring the stiffness of porous thin films as long as the indentation depths are small enough to avoid the substrate effect or if the substrate effect is properly accounted for.

IV. NEW TECHNIQUE FOR MEASURING MECHANICAL PROPERTIES OF POROUS MATERIALS BY NANOINDENTATION

The procedure for determining σ_y^D and σ_y^P in Sec. III. A requires an inverse analysis based on the finite element method. The question then arises if it is possible to correlate these quantities directly with the porosity and nanoindentation hardness of the porous material. For a bulk porous material with Young's modulus E^P and dense yield stress σ_y^D, dimensional analysis dictates that the normalized hardness measured is given by

$$c^P = \frac{H_b^P}{\sigma_y^D} = F\left[f, \frac{E_b^P}{\sigma_y^D}\right] \quad , \tag{9}$$

independent of indentation depth. The normalized hardness c^P is plotted as a function of indentation depth δ in Fig. 9(a) for several combinations of f and E^P/σ_y^D. For very shallow indentations, there is a slight variation of hardness with indentation depth. This is caused by the

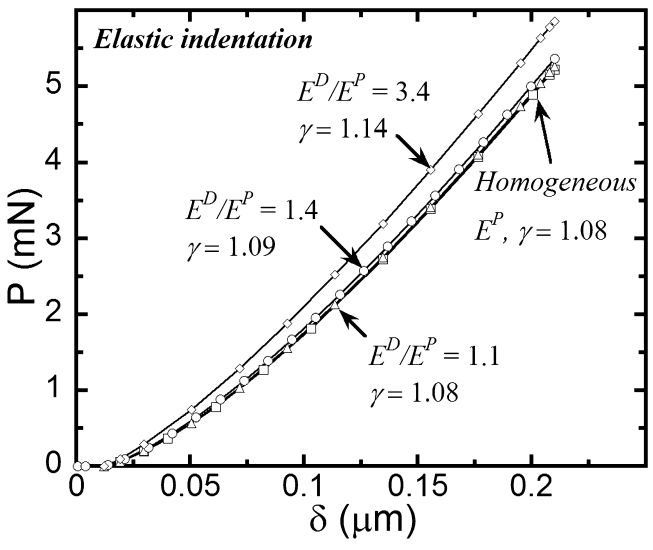

FIG. 8. FEM results show that the effect of porosity on indentation modulus is relatively small. Here γ is the normalized contact stiffness, $S/(2M\sqrt{A/\pi})$.

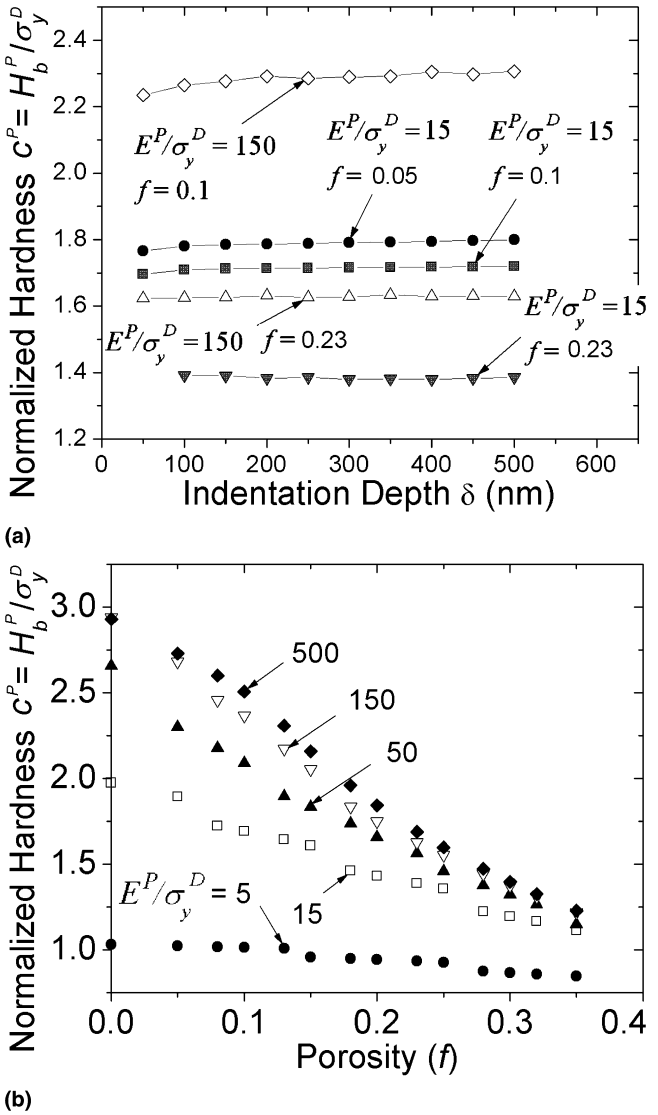

FIG. 9. (a) Normalized hardness as a function of indentation depth; (b) normalized hardness obtained with a Berkovich tip as a function of yield strain and porosity; this map can be used to calculate the dense yield stress from a hardness test.

finite curvature of the indenter tip used in the finite element simulation. For these shallow indentations, the plastic zone is not yet fully developed. Once the indentation depth exceeds 100 nm, however, the effect of the tip curvature is negligible. The deformation field under the indenter becomes self-similar and the hardness is independent of indentation depth. Therefore, the normalized hardness of a bulk porous material can be expressed as a function of just two parameters, the porosity and the yield strain of the dense material, as illustrated in Fig. 9(b). Thus, the dense yield stress σ_y^D of a material of known porosity and stiffness can be obtained from a nanoindentation experiment through use of Fig. 9(b). For a thin film on a substrate, the substrate effect must of course be corrected for first.

In summary, we propose the following approach to determine the mechanical properties (E,σ_y) of a porous thin film using nanoindentation:

(i) For a thin film of thickness h and porosity f, perform a nanoindentation experiment with indentation depth $\delta < h$ to obtain the hardness $H = P/A$ and indentation modulus $M = \sqrt{\pi}S/(2\gamma\sqrt{A})$ of the thin film. Both quantities are depth-dependent.

(ii) Obtain the intrinsic hardness H_b^P and indentation modulus M_b^P for the porous film independent of the substrate using the hardness and stiffness maps in Ref. 14 (compare Fig. 2). Young's modulus E^P of the porous film can be calculated from Eq. (4), if Poisson's ratio is known.

(iii) The yield stress of the matrix material, σ_y^D, can then be deduced from Fig. 9(b); the yield stress of the porous material, σ_y^P, is obtained from Fig. 7.

V. COMPARISON WITH EXPERIMENTAL RESULTS

Table I tabulates the experimental values of the modulus and yield stress of the dense and porous polymer films measured by nanoindentation and the bulge test. The moduli obtained from nanoindentation are systematically higher than those obtained from the bulge test for both dense and porous films. Since densification has no significant effect on the stiffness measurement, this difference can be attributed directly to the effect of the substrate in the nanoindentation measurements. According to the stiffness correction map in Fig. 2(b), the Si substrate increases the indentation modulus by approximately 20%, in good agreement with the experimental results.

To compare the yield stress of the polymer films obtained using the two different techniques, the approach proposed in Sec. IV is used to convert the experimental hardness values to yield stresses. For the fully dense polymer films, the conversion coefficient is found to be approximately 2.0, while for films with a porosity of 23%, it is 1.4 [see Fig. 9(b)]. Thus the hardness of the fully dense film corresponds to a yield stress of 115 MPa for the dense polymer; the hardness of the porous film leads to a value of 113 MPa for σ_y^D. The agreement between both measurements is quite remarkable. The results of the inverse analysis are consistent with the direct simulations in Sec. III. D. Furthermore, the nanoindentation measurements are in good agreement with the yield stress of 93 MPa obtained from the bulge test experiments on the fully dense film. Based on the nanoindentation experiments, the yield stress of the porous film is found to be approximately 86 MPa. The bulge test experiments only provide a lower bound of 55 MPa for the yield stress of the porous film, because all porous membranes ruptured in the linear elastic range before plastic deformation could take place. The good agreement between the experimental results obtained using nanoindentation and bulge testing validates the proposed analysis.

VI. CONCLUSION

We have analyzed the elastic-plastic indentation of porous materials using the Gurson model for solids that contain voids that are roughly spherical in shape. Finite element calculations using this model show that densification of the porous material occurs in a region immediately below the indenter. Densification has a significant impact on the hardness value obtained from indentation. The impact on the indentation modulus, by contrast, is insignificant. The computational results are in good agreement with experimental data obtained for a fully dense and a porous low-k dielectric coating with both nanoindentation and bulge test measurements. Based on the computational model, a new methodology is proposed for measuring the elastic-plastic properties of porous thin films using nanoindentation. This new approach extends the applicability of nanoindentation to porous materials and makes it possible to extract meaningful results from indentation measurements on porous solids.

ACKNOWLEDGMENTS

The work of Xi Chen is supported by National Science Foundation CMS-0407743. Joost Vlassak and Yong Xiang acknowledge financial support from National Science Foundation DMR-0213805 and from the Semiconductor Research Corporation (Task ID 12920.010).

REFERENCES

1. H.B. Huang and F. Spaepen: Tensile testing of free-standing Cu, Ag and Al thin films and Ag/Cu multilayers. *Acta Mater.* **48,** 3261 (2000).
2. Y. Xiang, X. Chen, and J.J. Vlassak: The plane-strain bulge test for thin films. *J. Mater. Res.* **20,** 2360 (2005).

3. J.J. Vlassak and W.D. Nix: A new bulge test technique for the determination of Young's modulus and Poisson's ratio of thin films. *J. Mater. Res.* **7,** 3242 (1992).
4. S.P. Baker and W.D. Nix: Mechanical properties of compositionally modulated Au-Ni thin films: Nanoindentation and microcantilever deflection experiments. *J. Mater. Res.* **9,** 3131 (1994).
5. T.P. Weihs, S. Hong, J.C. Bravman, and W.D. Nix: Mechanical deflection of cantilever microbeams—A new technique for testing the mechanical-properties of thin films. *J. Mater. Res.* **13,** 931 (1998).
6. S.P. Baker, A. Kretschmann, and E. Arzt: Thermomechanical behavior of different texture components in Cu thin films. *Acta Mater.* **49,** 2145 (2001).
7. R.M. Keller, S.P. Baker, and E. Arzt: Stress-temperature behaviour of unpassivated thin copper films. *Acta Mater.* **47,** 415 (1999).
8. W.C. Oliver and G.M. Pharr: An improved technique for determining hardness and elastic-modulus using load and displacement sensing indentation experiments. *J. Mater. Res.* **7,** 1564 (1992).
9. M.F. Doerner and W.D. Nix: A method for interpreting the data from depth-sensing indentation instruments. *J. Mater. Res.* **1,** 601 (1986).
10. G.M. Pharr: Measurement of mechanical properties by ultra-low-load indentation. *Mater. Sci. Eng. A* **253,** 151 (1998).
11. G.M. Pharr and A. Bolshakov: Understanding nanoindentation unloading curves. *J. Mater. Res.* **17,** 2660 (2002).
12. K.L. Johnson: *Contact Mechanics* (Cambridge University Press, Cambridge, UK, 1985).
13. J.C. Hay, A. Bolshakov, and G.M. Pharr: A critical examination of the fundamental relations used in the analysis of nanoindentation data. *J. Mater. Res.* **14,** 2296 (1999).
14. X. Chen and J.J. Vlassak: Numerical study on the measurement of thin film mechanical properties by means of nanoindentation. *J. Mater. Res.* **16,** 2974 (2001).
15. J.J. Vlassak and W.D. Nix: Measuring the elastic properties of anisotropic materials by means of indentation experiments. *J. Mech. Phys. Solids* **42,** 1223 (1994).
16. D. Tabor: *The Hardness of Metals* (Clarendon Press, Oxford, UK, 1951).
17. R. Saha and W.D. Nix: Effects of the substrate on the determination of thin film mechanical properties by nanoindentation. *Acta Mater.* **50,** 23 (2002).
18. N.A. Fleck, H. Otoyo, and A. Needleman: Indentation on porous solids. *Int. J. Solids Struct.* **29,** 1613 (1992).
19. A.A. Volinsky, J.B. Vella, and W.W. Gerberich: Fracture toughness, adhesion and mechanical properties of low-K dielectric thin films measured by nanoindentation. *Thin Solid Films* **429,** 201 (2003).
20. X. Chen, R. Wang, N. Yao, A.G. Evans, J.W. Hutchinson, and R.W. Bruce: Foreign object damage in a thermal barrier system: Mechanisms and simulations. *Mater. Sci. Eng. A* **352,** 221 (2003).
21. X. Chen, M.Y. He, I. Spitsberg, N.A. Fleck, J.W. Hutchinson, and A.G. Evans: Mechanisms governing the high temperature erosion of thermal-barrier coatings used in gas turbines. *Wear* **256,** 735 (2004).
22. X. Chen, J.W. Hutchinson, and A.G. Evans: Simulation of the high temperature impression of thermal-barrier coatings with columnar microstructure. *Acta Mater.* **52,** 565 (2004).
23. A.L. Gurson: Continuum theory of ductile rupture by void nucleation and growth. I. Yield criteria and flow rules for porous ductile media. *J. Eng. Mater. Technol.* **99,** 2 (1977).
24. Y. Xiang, X. Chen, T.Y. Tsui, J.I. Jang and J.J. Vlassak: Mechanical properties of porous and fully dense low-κ dielectric thin films measured by means of nanoindentation and the plane-strain bulge test technique. *J. Mater. Res.* **21,** 386 (2006).
25. H. Bückle: Use of hardness test to determine other material properties, in *The Science of Hardness Testing and Its Research Applications*, edited by J.W. Westbrook and H. Conrad (American Society for Metals, Metals Park, OH, 1971), p. 453
26. ABAQUS 5.8 User's Manual (ABAQUS Inc., Pawtucket, RI, 1998).
27. S.D. Mesarovic and N.A. Fleck: Spherical indentation of elastic-plastic solids. *Proc. R. Soc. London* **A455,** 2707 (1999).